Rapid charging of a two-qubit quantum battery by transverse field amplitude and phase control

Vasileios Evangelakos, Emmanuel Paspalakis and Dionisis Stefanatos*

E-mail: *dionisis@post.harvard.edu
Materials Science Department, School of Natural Sciences, University of Patras, Patras 26504, Greece

January 2025

Abstract. We consider a quantum battery composed of a pair of qubits coupled with an Ising interaction in the usual NMR framework, where the longitudinal applied field is constant and the time-dependent variables controlling the system are the amplitude and phase of the transverse field, and use optimal control to derive fast charging protocols. We study both the cases where the Ising coupling is weaker and stronger than the longitudinal field. In the first case, where the lowest-energy state of the system is the spin-down state, the optimal charging protocol stipulates the transverse field amplitude to be constant and equal to its maximum allowed value, while the minimum time for full charging of the battery tends to zero as this maximum bound increases. In the second case, where the lowest-energy state is a maximally entangled Bell state, the optimal charging protocol includes a time interval where the transverse field amplitude is zero and its phase is immaterial, corresponding to singular control. In this case, the quantum battery can be charged with higher levels of stored energy, while the minimum time for full charging tends to a nonzero limit proportional to the inverse Ising interaction, as the maximum bound of the control amplitude increases. We analyze intuitively and quantitatively the distinct behavior of the two cases and additionally use the dynamical Lie algebra of the system to elucidate the presence of a singular arc in the optimal pulse-sequence in the second case. The discovered interplay between the quantum battery parameters, the stored energy and the minimum time for full charging, provides great flexibility for optimizing the performance of the device according to the operating constraints. The valuable insights gained regarding the design of quantum batteries is expected to find immediate applications in modern quantum science and technology, while we aim to extend the proposed methods to larger spin chains.

1. Introduction

Quantum batteries (QBs) [1, 2] are a rapidly evolving concept in quantum technology, with the potential to outperform classical batteries in energy storage and retrieval at microscopic scales due to their reliance on inherently quantum mechanical phenomena, such as superposition and entanglement [2], as highlighted in recent theoretical studies

[3, 4, 5, 6, 7]. A wide variety of QB models have been proposed, ranging from simple few-level systems to complex many-body architectures, including spin chains, quantum oscillators, and interacting systems such as the Su-Schrieffer-Heeger and Sachdev-Ye-Kitaev models [8, 9, 10, 11, 12, 13, 14, 15, 16, 17, 18, 19, 20, 21, 22, 23, 24, 25, 26, 27, 28, 29, 30, 31, 32, 33, 34, 35, 36, 37, 38, 39, 40, 41, 42, 43, 44, 45, 46, 47, 48, 49, 50]. Experimental efforts have also begun to demonstrate QB prototypes on platforms such as superconductors [37], quantum dots [38], organic microcavities [39], and nuclear spin systems [29].

A crucial aspect of quantum batteries (QBs) is the design of efficient charging protocols to maximize the energy stored within the battery. Various quantum control techniques have been proposed to achieve this goal [51]. For instance, stimulated Raman adiabatic passage (STIRAP) [52, 53] has been employed to charge three-level QBs in both open [12] and closed [40] system configurations. Adiabatic passage has also been applied to non-interacting two-qubit systems [15]. Shortcuts to adiabaticity [54] have been utilized to accelerate charging processes across different models, including simple few-level setups [41, 42] as well as more complicated ones like the Lipkin-Meshkov-Glick system [43]. A related approach, the quantum adiabatic brachistochrone method, has been used experimentally in superconducting qutrit QBs [37]. Strong-pulse protocols have enabled rapid charging in many-body QB [44], while the quantum speed limit formalism has provided tighter bounds on the achievable charging times [55, 56]. Recently, optimal control theory [57, 58, 59, 60, 61] has been employed to derive optimal charging drives for qubit-based QBs [46, 47], numerical optimal control has been applied to coupled oscillator systems [48], while reinforcement learning optimization has been used to efficiently charge a Dicke quantum battery [49] and a cavity-Heisenberg spin-chain QB [50], highlighting the versatility of control techniques in enhancing QB performance.

In our recent work [47] we considered a pair of spin-1/2 particles coupled through an Ising interaction in the usual NMR framework, where the longitudinal applied field is fixed and the transverse field is used to control the system. We restricted our analysis to the case where the Ising coupling is weaker than the constant longitudinal field, so the spin-down state is the lowest energy state of the system, and used the transverse field amplitude as a control function, similarly to other studies [44, 46]. We derived optimal protocols for the fast charging of the QB, from the spin-down to the spin-up state. Here, we make a two-fold extension of our previous work. First, we use the phase of the transverse field as an extra control variable. This expanded control framework introduces new dynamical pathways and allows for the possibility of faster charging, as the phase modulation provides an extra degree of freedom. Second, we also study the case where the Ising interaction is stronger than the longitudinal field, so the lowest-energy state of the system is a maximally entangled Bell state, and show that, when starting from this state, *higher levels* of stored energy can be achieved in the QB. With the inclusion of phase control, the optimal charging protocol when the Ising coupling is weaker than the constant longitudinal field dictates that the transverse field amplitude is kept fixed

to its maximum allowed value. The minimum time for full charging of the QB tends to zero as this maximum bound increases. On the other hand, when the Ising interaction is stronger than the constant longitudinal field, the optimal charging protocol includes a time interval where the transverse field amplitude is zero and its phase is immaterial, corresponding to a so-called *singular* control. In this case, as the maximum bound on the control amplitude increases, the minimum time for full charging tends to a nonzero limit, which is is proportional to the inverse Ising coupling. We explain both intuitively and quantitatively the different behaviors observed in the two cases. We also employ the dynamical Lie algebra of the system to explain the presence of a singular arc in the optimal pulse-sequence in the case of stronger Ising interaction. The revealed interplay between system parameters, stored energy and charging time enables the performance optimization of the QB depending on the operating constraints.

While the present work focuses on a pair of spins, in the near future we plan to extend the methods introduced here to spin chains with three or more spins. Towards this goal, we may exploit the TorchQC framework for efficiently integrating machine and deep learning methods in quantum dynamics and control [62], recently developed by our group. Additionally, studying the role of phase-modulated controls in enhancing robustness against environmental noise and imperfections offers intriguing possibilities for future exploration. Investigating these aspects could provide valuable insights into the design of QBs that are both efficient and noise-resilient, particularly in experimental platforms where noise and decoherence are prevalent. The current findings contribute to the broader understanding of multi-parameter control in quantum batteries and lay the groundwork for more scalable and robust designs, potentially impacting modern quantum science and technology.

The paper is structured as follows. In section 2 we present the QB under study and formulate its charging in terms of optimal control. In sections 3 and 4 we derive optimal charging protocols for the cases where the Ising coupling is respectively weaker or stronger than the longitudinal field. In section 5 we use the dynamical Lie algebra of the system to understand how the different charging protocols for the two cases arise, while the article closes with section 6.

2. Optimal charging of an Ising two-qubit quantum battery

Consider an Ising spin-chain with N spins-1/2 in the standard NMR framework, with a constant longitudinal magnetic field and time-dependent transverse fields serving as the control functions, described by the Hamiltonian ($\hbar = 1$) [63]

$$\hat{H}(t) = \hat{H}_0 + \hat{H}_1(t) \tag{1}$$

with

$$\hat{H}_0 \quad = \Omega_z \sum_{n=1}^{N} \sigma_{nz} + J \sum_{1 \le n < n' \le N} \sigma_{nz}\sigma_{n'z}, \tag{2a}$$

$$\hat{H}_1(t) = \Omega_x(t) \sum_{n=1}^{N} \sigma_{nx} + \Omega_y(t) \sum_{n=1}^{N} \sigma_{ny}, \tag{2b}$$

where J is the Ising interaction, Ω_z the constant longitudinal field and $\Omega_x(t), \Omega_y(t)$ the transverse control fields. In this work we concentrate on the case with $N = 2$, corresponding to a quantum battery composed of a pair of coupled qubits.

Charging of this quantum battery corresponds to transferring population from the initial state $|\psi(0)\rangle$, which is usually taken to be the ground state, to the excited states such that at the final time T the stored energy is maximized

$$\begin{aligned} \Delta E &= E(T) - E(0) \\ &= \langle\psi(T)| \hat{H}_0 |\psi(T)\rangle - \langle\psi(0)| \hat{H}_0 |\psi(0)\rangle . \end{aligned} \tag{3}$$

In this work we use transverse control fields with time-dependent amplitude $\Omega(t)$ and phase $\phi(t)$, and carrier frequency ω_c

$$\Omega_x(t) = \Omega(t) \cos[\omega_c t + \phi(t)], \tag{4a}$$

$$\Omega_y(t) = -\Omega(t) \sin[\omega_c t + \phi(t)]. \tag{4b}$$

We consider that the amplitude is bounded by a maximum value Ω_0

$$0 \leq \Omega(t) \leq \Omega_0, \tag{5}$$

and under this restriction we find $\Omega(t), \phi(t)$ maximizing the stored energy (3) for a given duration T.

For $N = 2$, Hamiltonian $\hat{H}_1$ couples the triplet states

$$|\psi_0\rangle = |00\rangle , \tag{6a}$$

$$|\psi_1\rangle = \frac{1}{\sqrt{2}} (|01\rangle + |10\rangle) , \tag{6b}$$

$$|\psi_2\rangle = |11\rangle , \tag{6c}$$

while the singlet state $|\phi\rangle = (|01\rangle - |10\rangle)/\sqrt{2}$ is decoupled [64]; note that $|0\rangle = (0\ 1)^T, |1\rangle = (1\ 0)^T$ are the individual spin-down and spin-up states, respectively. Let

$$|\psi(t)\rangle = a_0(t) |\psi_0\rangle + a_1(t) |\psi_1\rangle + a_2(t) |\psi_2\rangle \tag{7}$$

be the representation of the system state on the triplet manifold, with $a_i, i = 0, 1, 2$ the corresponding probability amplitudes. Schrödinger equation

$$i \frac{\partial}{\partial t} |\psi(t)\rangle = \hat{H} |\psi(t)\rangle \tag{8}$$

leads to equation

$$i \frac{d\mathbf{a}}{dt} = \begin{bmatrix} J - 2\Omega_z & \sqrt{2}(\Omega_x - i\Omega_y) & 0 \\ \sqrt{2}(\Omega_x + i\Omega_y) & -J & \sqrt{2}(\Omega_x - i\Omega_y) \\ 0 & \sqrt{2}(\Omega_x + i\Omega_y) & J + 2\Omega_z \end{bmatrix} \mathbf{a} \tag{9}$$

for the state vector $\mathbf{a} = (a_0\ a_1\ a_2)^T$. The diagonal terms express the eigenenergies of the triplet states and obviously the ground state of the battery depends on the ratio

$$\chi = \frac{J}{\Omega_z}. \tag{10}$$

We thus distinguish the following two cases.

3. Case $J < \Omega_z$

In this case, the ground state is the spin-down state $|\psi_0\rangle$. Using it as the initial state $|\psi(0)\rangle = |\psi_0\rangle$ in Eq. (3), we obtain the following expression for the stored energy in terms of the final populations of the spin-up and spin-down states

$$\frac{\Delta E}{\Omega_z} = 2\left[(1-\chi)(1-|a_0(T)|^2) + (1+\chi)|a_2(T)|^2\right], \tag{11}$$

where $\chi = J/\Omega_z < 1$ and for the closed system under study we have used $|a_1(T)|^2 = 1 - |a_0(T)|^2 - |a_2(T)|^2$. The maximum stored energy is $\Delta E_{max} = 4\Omega_z$.

By making the population preserving transformation

$$c_0 = a_0 e^{i(J-\omega_c)t}, \tag{12a}$$

$$c_1 = a_1 e^{iJt}, \tag{12b}$$

$$c_2 = a_2 e^{i(J+\omega_c)t}, \tag{12c}$$

we obtain for $\mathbf{c} = (c_0\ c_1\ c_2)^T$ the equation

$$i\frac{d\mathbf{c}}{dt} = \begin{bmatrix} \omega_c - 2\Omega_z & \sqrt{2}\Omega(t)e^{i\phi(t)} & 0 \\ \sqrt{2}\Omega(t)e^{-i\phi(t)} & -2J & \sqrt{2}\Omega(t)e^{i\phi(t)} \\ 0 & \sqrt{2}\Omega(t)e^{-i\phi(t)} & 2\Omega_z - \omega_c \end{bmatrix} \mathbf{c}. \tag{13}$$

We would like starting from state $|\psi_0\rangle$ to maximize the stored energy and since the spin-up state $|\psi_2\rangle$ has the highest energy we choose the carrier frequency as $\omega_c = 2\Omega_z$, ending up with the equation

$$i\frac{d\mathbf{c}}{dt} = \begin{bmatrix} 0 & \sqrt{2}\Omega(t)e^{i\phi(t)} & 0 \\ \sqrt{2}\Omega(t)e^{-i\phi(t)} & -2J & \sqrt{2}\Omega(t)e^{i\phi(t)} \\ 0 & \sqrt{2}\Omega(t)e^{-i\phi(t)} & 0 \end{bmatrix} \mathbf{c}. \tag{14}$$

Note that this equation may describe the time evolution of populations of exciton and biexciton states in a semiconductor quantum dot, see for example Ref. [65].

In our recent work [47] we solved the problem of maximizing the stored energy for fixed charging duration T when $J < \Omega_z$, thus the battery starts from the spin-down state, for the cases where the control phase is allowed to take only the value $\phi = 0$ or the two values $\phi = 0, \pi$. Since we were interested in the fast charging of the battery, we considered relatively strong values of the maximum control amplitude, $\Omega_0 > \sqrt{3}J/2$. We found that, although for short durations a single On pulse $\Omega(t) = \Omega_0$ with any of the allowed phases is optimal, for longer durations, including those needed for full charging of the battery (maximum stored energy), a pulse-sequence of the form bang-singular-bang is optimal. The two bang pulses in the optimal sequence are On pulses, with different durations and the same phase when $\phi = 0$ and same duration but different phases when the values $\phi = 0, \pi$ are permitted. The intermediate singular pulse is an Off pulse $\Omega(t) = 0$ with different duration than a bang Off pulse. We also found that

the minimum necessary duration for full charging, for the cases $\phi = 0$ and $\phi = 0, \pi$, is given by the transcendental equations

$$n_z \tan JT + \tan\left[\frac{\omega(\pi - 2JT)}{2J}\right] = 0, \tag{15a}$$

$$\tan JT + n_z \tan\left[\frac{\omega(\pi - 2JT)}{2J}\right] = 0, \tag{15b}$$

where

$$\omega = \sqrt{4\Omega_0^2 + J^2}, \quad n_z = \frac{J}{\omega}. \tag{16}$$

Note that Eqs. (15a),(15b) are slightly different from the corresponding equations in Ref. [47] since here we use different scaling for Ω_k, $k = x, y, z$ and J. In Fig. 1 we plot the minimum duration obtained from Eqs. (15a),(15b) as a function of the maximum control amplitude, with blue dashed line for the case where $\phi = 0$, Eq. (15a), and with red solid line for the case where the phase can take the values $\phi = 0, \pi$, Eq. (15b). We observe that for large values of Ω_0 both curves tend to the limiting value $\pi/2J$.

In the present work, we solve the problem of maximizing the stored energy (11) using as an additional control the time-dependent phase $\phi(t)$ of the control field. We use the Scrödinger equation (14) as state equation, so $|\psi(t)\rangle = [c_0(t), c_1(t), c_2(t)]^T$. If $|\lambda(t)\rangle = [\lambda_0(t), \lambda_1(t), \lambda_2(t)]^T$ denotes the adjoint ket state then, using the standard control formalism as applied to quantum systems [66], the control Hamiltonian is

$$\begin{aligned} H_c &= \Re(\langle\lambda|\dot{\psi}\rangle), \\ &= \sqrt{2}\Omega(A\sin\phi + B\cos\phi) + JC, \end{aligned} \tag{17}$$

where

$$\begin{aligned} A &= \Re(c_1)\,\Re(\lambda_0 - \lambda_2) + \Im(c_1)\,\Im(\lambda_0 - \lambda_2) + \Re(\lambda_1)\,\Re(c_2 - c_0) + \Im(\lambda_1)\,\Im(c_2 - c_0), \\ B &= -\Re(c_1)\,\Im(\lambda_0 + \lambda_2) + \Im(c_1)\,\Re(\lambda_0 + \lambda_2) + \Re(\lambda_1)\,\Im(c_0 + c_2) - \Im(\lambda_1)\,\Re(c_0 + c_2), \\ C &= 2\Re(c_1)\,\Im(\lambda_1) - 2\Im(c_1)\,\Re(\lambda_1) \end{aligned} \tag{18}$$

and $\Re, \Im$ denote real and imaginary parts, respectively.

If we define the derivative with respect to $|\psi\rangle$ as

$$\frac{\partial}{\partial|\psi\rangle} = \frac{1}{2}\left(\frac{\partial}{\partial\Re(|\psi\rangle)} - i\frac{\partial}{\partial\Im(|\psi\rangle)}\right), \tag{19}$$

then $|\psi\rangle, |\lambda\rangle$ satisfy the pair of Hamilton's equation

$$\begin{aligned} |\dot{\psi}\rangle &= 2\frac{\partial H_c}{\partial\langle\lambda|}, \\ \langle\dot{\lambda}| &= -2\frac{\partial H_c}{\partial|\psi\rangle}, \end{aligned} \tag{20}$$

The first equation gives Eq. (14) as expected, while the second one leads to a similar equation for $\langle\lambda|$

$$\langle\dot{\lambda}| = i\langle\lambda|\hat{H}, \tag{21}$$

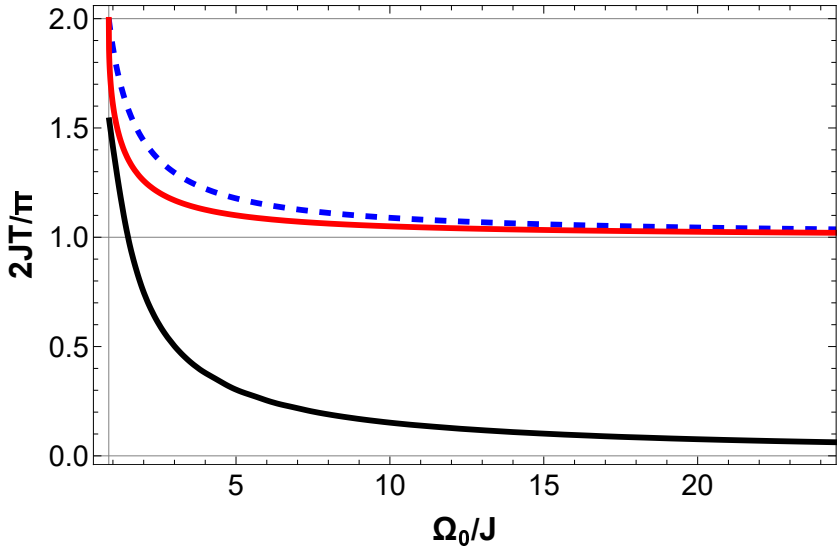

Figure 1: Minimum durations for full charging a quantum battery with ratio $\chi = J/\Omega_z = 1/2$ when the transverse control field amplitude is constrained as $0 \leq \Omega(t) \leq \Omega_0$, for the cases where the field phase is restricted to the value $\phi = 0$ (blue dashed curve), or the values $\phi = 0, \pi$ (red solid curve), or is allowed to be time-dependent $\phi(t)$ (black solid curve).

where $\hat{H}$ is the Hermitian matrix on the right hand side of Eq. (14). The adjoint variables should also satisfy the terminal condition

$$\langle \lambda(T)| = 2\frac{\partial\left(\frac{\Delta E(T)}{\Omega_z}\right)}{\partial\,|\psi(T)\rangle}, \tag{22}$$

which leads to

$$|\lambda(T)\rangle = \begin{bmatrix} 4(\chi-1)c_0(T) \\ 0 \\ 4(\chi+1)c_2(T) \end{bmatrix}. \tag{23}$$

According to Pontryagin's maximum principle [57, 58], the optimal controls $\Omega^*(t), \phi^*(t)$ are selected to maximize the control Hamiltonian (17). Since there are no restrictions on ϕ, we have when $\Omega(t) \neq 0$

$$\frac{\partial H_c}{\partial \phi}\Big|_{\phi=\phi^*} = 0 \Rightarrow \tan\phi^* = \frac{A}{B}, \tag{24}$$

which leads to

$$H_c = \Omega\sqrt{2(A^2+B^2)} + CJ. \tag{25}$$

Observe from Eq. (25) that if either $A \neq 0$ or $B \neq 0$ then the optimal control amplitude maximizing H_c is $\Omega^*(t) = \Omega_0$. If $A = B = 0$ for a finite time interval then maximum principle provides a priori no information about the optimal Ω. In this case Ω^* can take any value in the interval $[0\ \Omega_0]$ and the corresponding optimal control is called singular. Particular attention should be paid to the intervals where $\Omega^*(t) = 0$, in which

case the phase is immaterial. In the next section we will clarify the mechanism under which optimal solutions containing such intervals emerge, while in section 5 we will further expand our understanding of this phenomenon using the dynamical Lie algebra generated by the system Hamiltonian.

For the present case, numerical optimal control indicates that $\Omega^*(t) = \Omega_0$ throughout the whole interval $[0\ T]$, no matter how large the maximum amplitude Ω_0 is. The optimal phase is determined by Eq. (24) and is actually a function of the components of state $|\psi\rangle$ and adjoint state $|\lambda\rangle$, see Eqs. (18) for A, B. In this case, Eqs. (14) and (21) along with the initial condition $|\psi(0)\rangle = |\psi_0\rangle$ for the state and the terminal condition (23) involving both the state and the adjoint, form a two-point boundary value problem. The optimal control solver finds numerically the adjoint state initial condition $|\lambda(0)\rangle$, which can then be used along with the state initial condition $|\psi(0)\rangle = |\psi_0\rangle$ to propagate Eqs. (14) and (21) forward in time, while the optimal phase is determined from Eq. (24).

We use numerical optimal control to solve the problem of full charging a quantum battery with ratio $\chi = J/\Omega_z = 1/2$ and various values of the maximum control amplitude Ω_0, and plot in Fig. 1 the minimum necessary duration for full charging versus Ω_0 (black solid curve). Observe that the time needed in this case is shorter than the previously studied cases with restricted control on phase ϕ. Furthermore, this time now approaches zero as Ω_0 increases, beating the $\pi/(2J)$ lower limit of the previous cases. We can understand how the zero time limit is approached by considering a delta pulse with amplitude $\Omega_0 \to \infty$, duration $T \to 0$ and constant phase ϕ. In this case, the J-term in Eq. (14) can be ignored and the solution of this equation becomes

$$c_0(T) = \frac{1}{2}(\cos 2\Omega_0 T + 1), \tag{26a}$$

$$c_1(T) = -\frac{ie^{-i\phi}}{\sqrt{2}} \sin 2\Omega_0 T, \tag{26b}$$

$$c_2(T) = \frac{e^{-2i\phi}}{2}(\cos 2\Omega_0 T - 1). \tag{26c}$$

If the pulse area is $\Omega_0 T = \pi/2$, then $|c_2(T)| = 1$ and the battery is fully charged within $T \to 0$.

In Figs. 2, 3, 4, 5, we present results regarding the full charging of the quantum battery with ratio $\chi = J/\Omega_z = 1/2$ and maximum control amplitude $\Omega_0/J = 1, 3, 6, 50$, respectively. For each case we display the optimal controls $\Omega(t), \phi(t)$ [subfigures (a), (b)], as well as the time evolution of the stored energy $\Delta E(t)$ [subfigure (c)] and the populations of the triplet states $|c_0(t)|^2, |c_1(t)|^2, |c_2(t)|^2$ [red, green and blue lines in subfigures (d)]. Observe that in all the cases the optimal amplitude is constant and equal to the maximum value $\Omega(t) = \Omega_0$, while the optimal phase has a similar shape with some slight differences at the beginning and end. This "cup" profile of the optimal phase persists even for large values of Ω_0, see f.e. Fig. 5(b) obtained for $\Omega_0/J = 50$. The time-dependent phase allows the full charging of the battery within a duration which tends to zero as Ω_0 increases, see the black curve in Fig. 1. On the contrary, in our

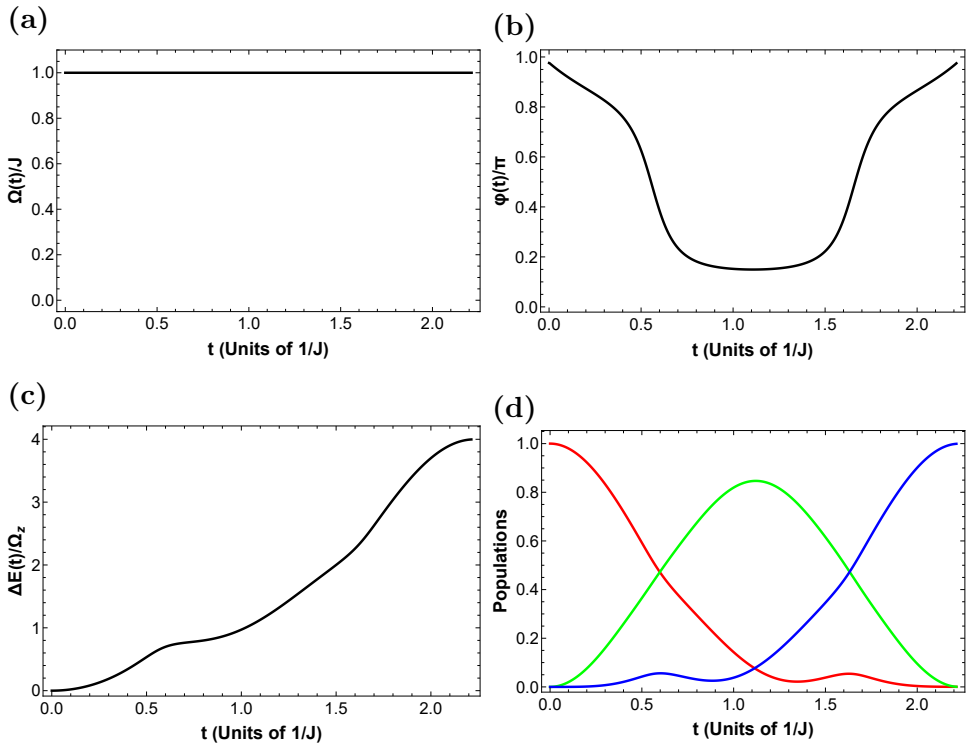

Figure 2: Optimal control amplitude (a) and phase (b), along with the corresponding time evolution of stored energy (c) and populations ($|c_0|^2$ red, $|c_1|^2$ green, $|c_2|^2$ blue) (d) for full charging in minimum time, when $\Omega_0/J = 1$ and $\chi = J/\Omega_z = 1/2$.

previous work [47] where ϕ was restricted to the values 0 or $0, \pi$, there was a finite time limit for full charging even for large Ω_0, see the red and blue curves tending to $\pi/(2J)$ in Fig. 1.

4. Case $J > \Omega_z$

In this case, the lowest energy state is $|\psi_1\rangle$. If we use it as the initial state $|\psi(0)\rangle = |\psi_1\rangle$ in Eq. (3), we find for the final stored energy the expression

$$\frac{\Delta E}{\Omega_z} = 2\left[(\chi - 1)(1 - |a_1(T)|^2) + 2|a_2(T)|^2\right], \tag{27}$$

where now $\chi = J/\Omega_z > 1$ and we have also used that $|a_0(T)|^2 = 1 - |a_1(T)|^2 - |a_2(T)|^2$. Now the maximum stored energy is $\Delta E_{max} = 2(\chi + 1)\Omega_z$, larger than the previous case since $\chi > 1$. This observation provides additional motivation for the investigation of this case.

By making the following transformation

$$c_0 = a_0 e^{-i(J+\omega_c)t}, \tag{28a}$$
$$c_1 = a_1 e^{-iJt}, \tag{28b}$$
$$c_2 = a_2 e^{-i(J-\omega_c)t}, \tag{28c}$$

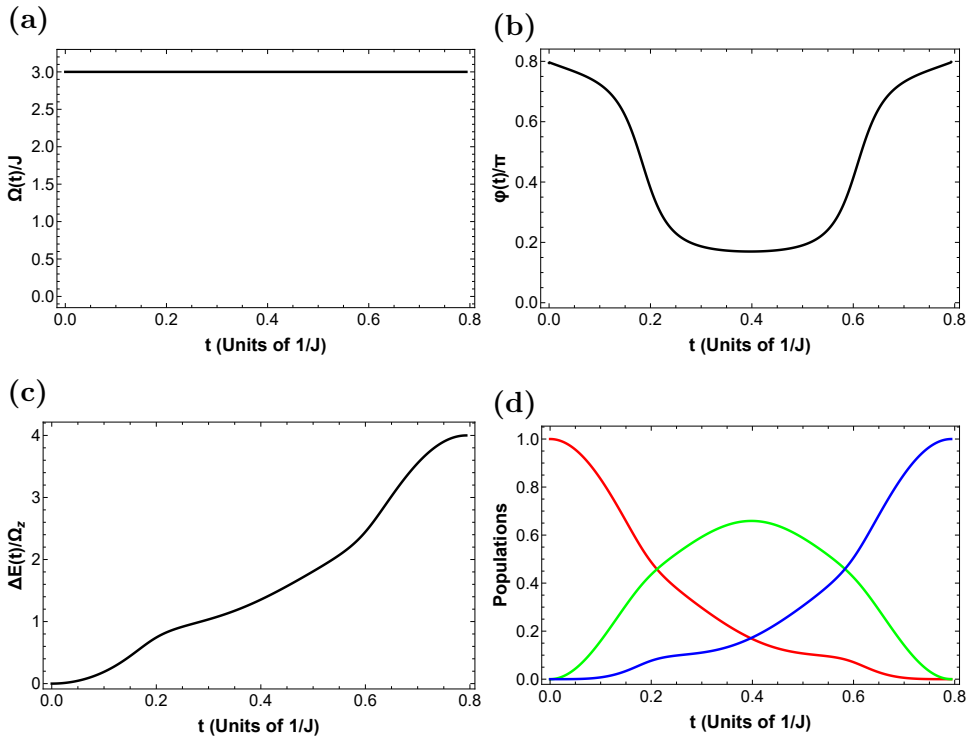

Figure 3: Optimal control amplitude (a) and phase (b), along with the corresponding time evolution of stored energy (c) and populations ($|c_0|^2$ red, $|c_1|^2$ green, $|c_2|^2$ blue) (d) for full charging in minimum time, when $\Omega_0/J = 3$ and $\chi = J/\Omega_z = 1/2$.

we find for $\mathbf{c} = (c_0\ c_1\ c_2)^T$ the equation

$$i\frac{d\mathbf{c}}{dt} = \begin{bmatrix} \omega_c + 2J - 2\Omega_z & \sqrt{2}\Omega(t)e^{i\phi(t)} & 0 \\ \sqrt{2}\Omega(t)e^{-i\phi(t)} & 0 & \sqrt{2}\Omega(t)e^{i\phi(t)} \\ 0 & \sqrt{2}\Omega(t)e^{-i\phi(t)} & 2J + 2\Omega_z - \omega_c \end{bmatrix} \mathbf{c}. \tag{29}$$

We want starting from $|\psi_1\rangle$ to maximize the stored energy and since the spin-up state $|\psi_2\rangle$ has the highest energy, we choose the carrier frequency as $\omega_c = 2\Omega_z + 2J$, ending up with the equation

$$i\frac{d\mathbf{c}}{dt} = \begin{bmatrix} 4J & \sqrt{2}\Omega(t)e^{i\phi(t)} & 0 \\ \sqrt{2}\Omega(t)e^{-i\phi(t)} & 0 & \sqrt{2}\Omega(t)e^{i\phi(t)} \\ 0 & \sqrt{2}\Omega(t)e^{-i\phi(t)} & 0 \end{bmatrix} \mathbf{c}. \tag{30}$$

Eq. (30) can be seen as describing two two-level systems with the same ground state $|\psi_1\rangle$ and excited states $|\psi_2\rangle$ and $|\psi_0\rangle$. The applied field appears to be on-resonance with the first two-level system, while out of resonance by an effective detuning $4J$ from the second. If the strength of the control field, as expressed by the maximum amplitude Ω_0, is not very large compared to the detuning, then the highest energy state $|\psi_2\rangle$ can be selectively excited.

The optimal control analysis of the previous section, expressed by Eqs. (17)-(25), is also carried here. Eq. (17) for the control Hamiltonian still holds, with the same A, B

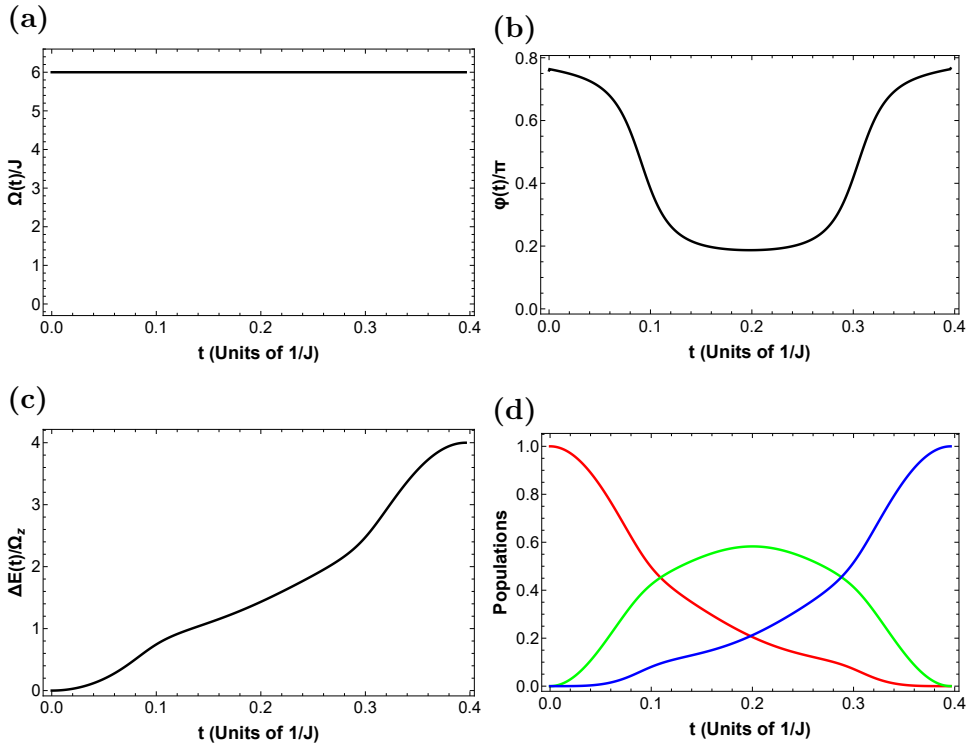

Figure 4: Optimal control amplitude (a) and phase (b), along with the corresponding time evolution of stored energy (c) and populations ($|c_0|^2$ red, $|c_1|^2$ green, $|c_2|^2$ blue) (d) for full charging in minimum time, when $\Omega_0/J = 6$ and $\chi = J/\Omega_z = 1/2$.

but different C given below

$$C = 4\Im\left(c_0\right)\Re\left(\lambda_0\right) - 4\Re\left(c_0\right)\Im\left(\lambda_0\right), \tag{31}$$

while the terminal condition for the adjoint state is also modified as follows

$$|\lambda(T)\rangle = \begin{bmatrix} 0 \\ 4(1-\chi)c_1(T) \\ 8c_2(T) \end{bmatrix}. \tag{32}$$

We use symbol J' to denote the coupling in Eq. (30) and consider the case $J' = 4J = 2\Omega_z$, where the symbol J is reserved for the coupling of the case presented in the previous section and is used here to normalize control amplitude and duration to facilitate comparison. We use numerical optimal control to solve the problem of full charging the quantum battery with ratio $\chi = J'/\Omega_z = 2$ and various values of the maximum control amplitude $\Omega_0/J = 1, 3, 4, 6$, with the corresponding results displayed in Figs. 6, 7, 8, 9, respectively. Observe that for smaller Ω_0 (Figs. 6 and 7), the optimal control amplitude attains its maximum value, as in the case of the previous section, while the time-dependence of the optimal phase changes appreciably. But for larger Ω_0 (Figs. 8 and 9), it appears an interval where the optimal control amplitude is zero, during which the phase is immaterial.

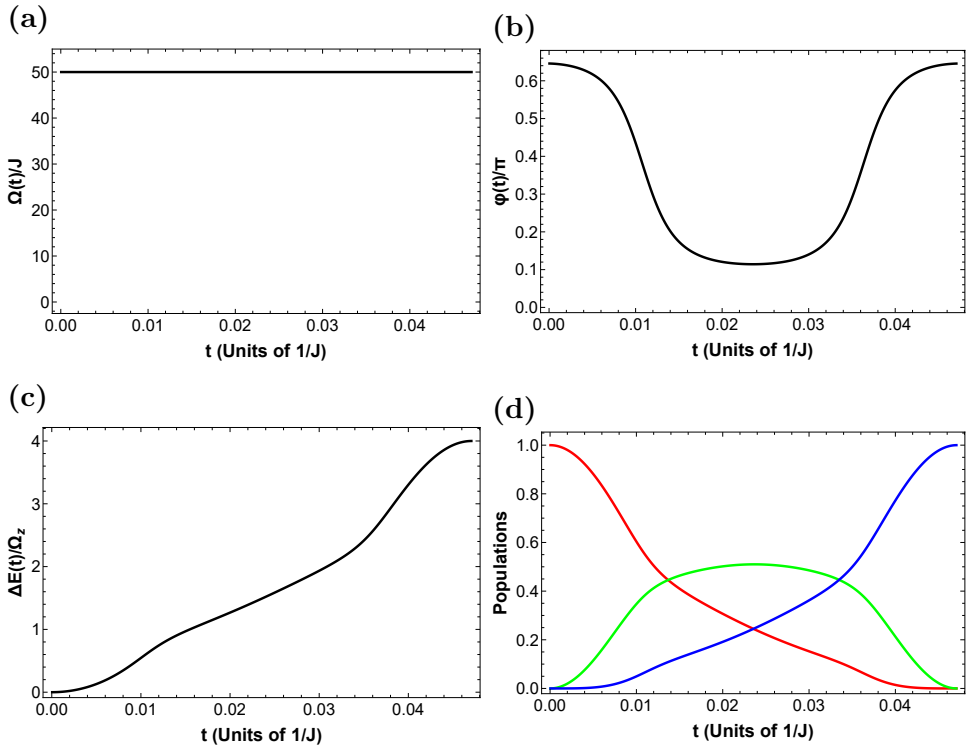

Figure 5: Optimal control amplitude (a) and phase (b), along with the corresponding time evolution of stored energy (c) and populations ($|c_0|^2$ red, $|c_1|^2$ green, $|c_2|^2$ blue) (d) for full charging in minimum time, when $\Omega_0/J = 50$ and $\chi = J/\Omega_z = 1/2$.

In Fig. 10(a) we display the minimum necessary duration for full charging of the quantum battery versus the maximum control amplitude Ω_0, for the case where $J' = 4J$ (red solid line). We observe that, as Ω_0 increases, this minimum time tends to a limiting value greater than zero. We also plot the minimum full charging duration versus Ω_0 for $J' = 5J$ (green solid line) and $J' = 6J$ (blue solid line), corresponding to larger values of ratio χ. We observe that, with increasing J', full charging is achieved faster, while the minimum time limit reached for larger Ω_0 is decreased. For comparison, we also display in the same figure (black solid line) the minimum full charging duration for the example with $J < \Omega_z$ presented in the previous section, which tends to zero with increasing Ω_0. It is clear that for smaller values of Ω_0, the battery with $J' > \Omega_z$ is charged faster. In addition, the maximum stored energy achieved is larger, $2(\chi + 1)\Omega_z > 4\Omega_z$ since $\chi > 1$. The full advantage of using batteries with $J' > \Omega_z$ for smaller Ω_0 becomes apparent in Fig. 10(b), where we show the charging power corresponding to the cases displayed in Fig. 10(a). The almost linear dependence of the charging power for $J < \Omega_z$ is attributed to that in this case $T \sim 1/\Omega_0$ for large Ω_0, as we explained in the previous section.

We can intuitively understand the observed behavior and especially the appearance of a zero control time interval and the finite minimum full charging duration as Ω_0 increases, using the Schrödinger equation (30). Note that when the control amplitude is $\Omega(t) = \Omega_0 \gg J'$, the effect of the detuning is screened and state $|\psi_2\rangle$ cannot be

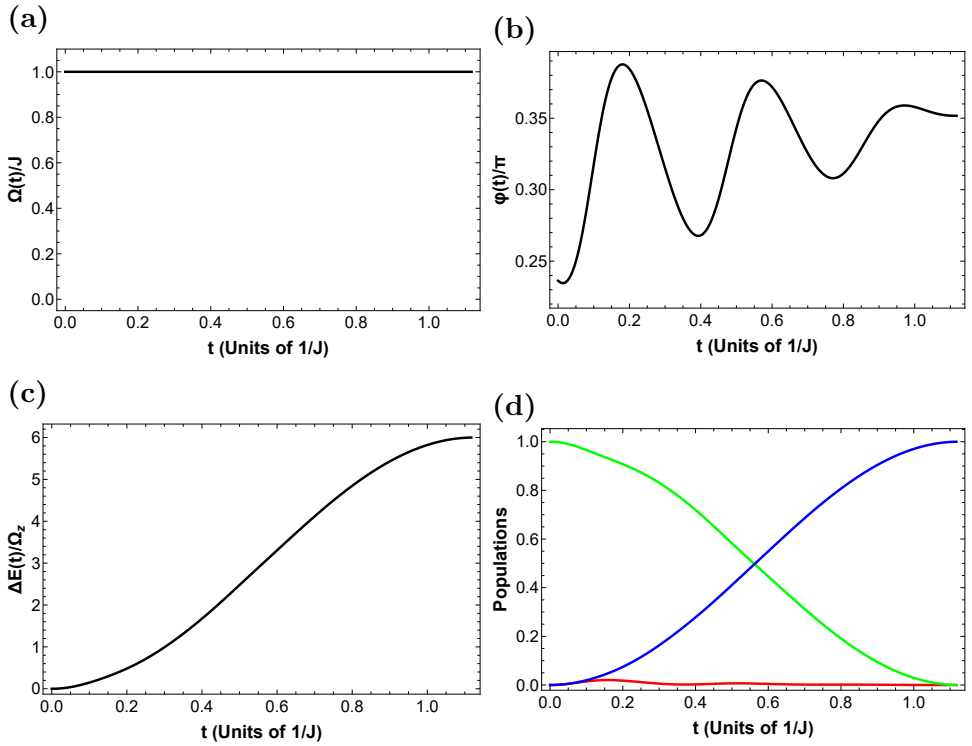

Figure 6: Optimal control amplitude (a) and phase (b), along with the corresponding time evolution of stored energy (c) and populations ($|c_0|^2$ red, $|c_1|^2$ green, $|c_2|^2$ blue) (d) for full charging in minimum time, when $\Omega_0/J = 1$ and $\chi = J'/\Omega_z = 2$.

selectively excited when starting from $|\psi_1\rangle$, since state $|\psi_0\rangle$ is also excited. This is additionally confirmed by evaluating the eigenvalues of the matrix in the right hand side of Eq. (30). The characteristic equation is

$$\left(\frac{E}{\Omega_0}\right)^3 - \frac{4J'}{\Omega_0}\left(\frac{E}{\Omega_0}\right)^2 - 2\frac{E}{\Omega_0} + \frac{4J'}{\Omega_0} = 0, \tag{33}$$

with solutions $E_0/\Omega_0 \approx 2J'/\Omega_0$ and $E_\pm/\Omega_0 \approx \pm\sqrt{2} + J'/\Omega_0$ to first order in J'/Ω_0, which tend to the values $E_0 \to 0$ and $E_\pm \to \pm\sqrt{2}\Omega_0$ in the limit $\Omega_0 \gg J'$. To resolve the levels $|\psi_2\rangle$ and $|\psi_0\rangle$ for large Ω_0, it is necessary to introduce a time interval where $\Omega(t) = 0$, during which only the J' term is active in Eq. (30). The resolution time is proportional to $1/J'$, as observed with the limiting durations in Fig. 10(a).

We next move to explain with a specific example how the segment $\Omega(t) = 0$ enters the optimal solution. We use a coupling in Eq. (30) equal to $J' = 4J = 2\Omega_z$ and consider a maximum control amplitude $\Omega_0 = 4J$, as in Fig. 8. The maximum stored energy for the above values is $\Delta E_{max} = 2(\chi + 1)\Omega_z = 12J$. In Fig. 11 we display the numerically obtained optimal controls $\Omega(t), \phi(t)$ for three durations $T = 0.29J^{-1}$ (first row), $T = 0.31J^{-1}$ (second row) and $T = 0.33J^{-1}$ (third row), which achieve stored energies at the final time $\Delta E/\Delta E_{max} = 97.14\%, 99.11\%, 99.95\%$, respectively. Observe that for the shorter duration (first row) the optimal controls resemble those displayed in the first row of Fig. 7, which achieve full charging for smaller $\Omega_0 = 3J$. But as the

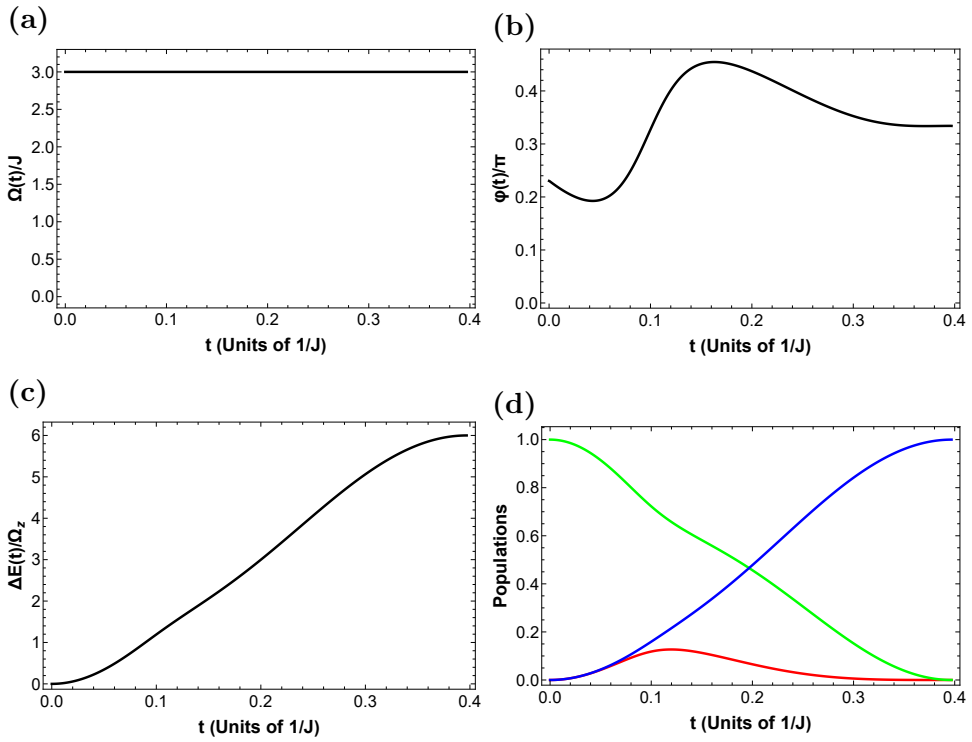

Figure 7: Optimal control amplitude (a) and phase (b), along with the corresponding time evolution of stored energy (c) and populations ($|c_0|^2$ red, $|c_1|^2$ green, $|c_2|^2$ blue) (d) for full charging in minimum time, when $\Omega_0/J = 3$ and $\chi = J'/\Omega_z = 2$.

duration increases (second raw) and higher charging levels are reached, the change in phase ϕ becomes more abrupt. A further increase in the duration (third row) which allows to approach full charging levels, leads to a discontinuity in ϕ and the development of a corresponding time interval where $\Omega(t) = 0$. From a control-theoretic point of view we can understand this behavior as follows. According to Pontryagin's maximum principle, for an autonomous control system (without explicit time dependence) like the one of Eq. (30), the control Hamiltonian (17) is constant throughout. Since the state and adjoint variables $\mathbf{c}, \lambda$ are continuous, coefficients A, B, C in expression (17) are also continuous. Then, the discontinuity in ϕ can be consistent with the constancy of H_c only when either $\Omega(t) = 0$ or $A = B = 0$. In the next section we use the dynamical Lie algebra of the system to show that the singular condition $A = B = 0$ also implies that $\Omega(t) = 0$.

Numerical optimal control indicates that, as the maximum control amplitude Ω_0 increases, the interval where $\Omega(t) = 0$ occupies a larger portion in the optimal pulse-sequence achieving full charging, compare f.e. Figs. 8(a) and 9(a). We use this observation to calculate the minimum duration for full charging, corresponding to the lower time limits in Fig. 10(a). In the limit $\Omega_0 \to \infty$ we expect the optimal pulse-sequence to consist of an initial delta pulse, followed by the interval of duration T where $\Omega(t) = 0$, and a final delta pulse. Let $\tau_1 \to 0$ denote the "duration" of the first delta

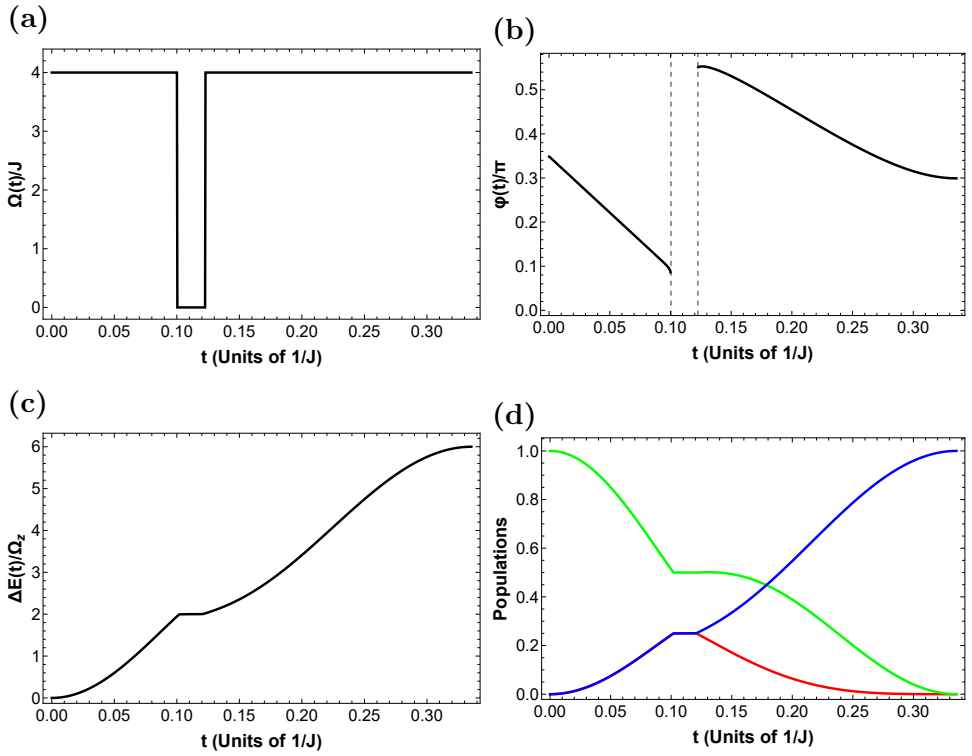

Figure 8: Optimal control amplitude (a) and phase (b), along with the corresponding time evolution of stored energy (c) and populations ($|c_0|^2$ red, $|c_1|^2$ green, $|c_2|^2$ blue) (d) for full charging in minimum time, when $\Omega_0/J = 4$ and $\chi = J'/\Omega_z = 2$.

pulse and ϕ_1 its constant phase, while define the angle $\theta_1 = 2\Omega_0\tau_1$. Using Eq. (30) we find immediately after the application of the pulse

$$c_0(0^+) = -\frac{i}{\sqrt{2}}\sin\theta_1, \tag{34a}$$

$$c_1(0^+) = e^{-i\phi_1}\cos\theta_1, \tag{34b}$$

$$c_2(0^+) = -\frac{ie^{-2i\phi_1}}{\sqrt{2}}\sin\theta_1. \tag{34c}$$

In the subsequent interval where $\Omega(t) = 0$, only the coupling term in Eq. (30) is active. Thus, if we set $\theta_2 = 4J'T$, we get

$$c_0(T^-) = c_0(0^+)e^{-i\theta_2}, \tag{35a}$$

$$c_1(T^-) = c_1(0^+), \tag{35b}$$

$$c_2(T^-) = c_2(0^+). \tag{35c}$$

Now let $\tau_2 \to 0$ denote the "duration" of the final delta pulse and ϕ_2 its constant phase, while define the angle $\theta_3 = 2\Omega_0\tau_2$ and the difference of the phases $\delta\phi = \phi_2 - \phi_1$. Then, Eq. (30) gives

$$c_0(T) = \frac{ie^{i\delta\phi}}{\sqrt{2}}\left\{\frac{1}{2}\sin\theta_1(1-\cos\theta_3)e^{i\delta\phi} - \frac{1}{2}\sin\theta_1(1+\cos\theta_3)e^{-i(\delta\phi+\theta_2)} - \cos\theta_1\sin\theta_3\right\},$$

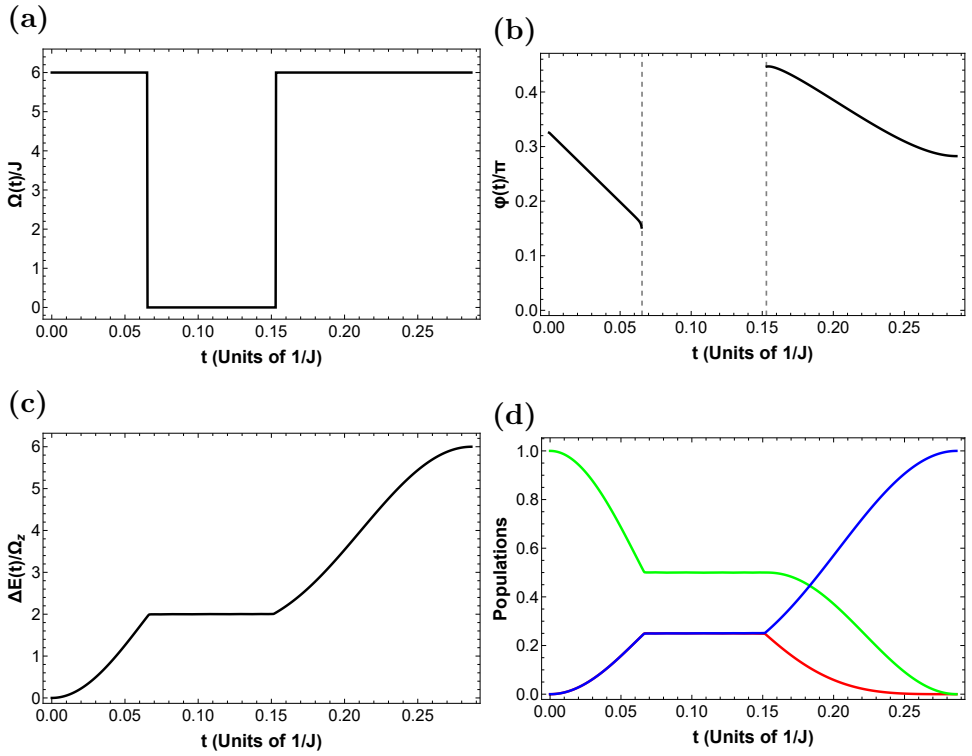

Figure 9: Optimal control amplitude (a) and phase (b), along with the corresponding time evolution of stored energy (c) and populations ($|c_0|^2$ red, $|c_1|^2$ green, $|c_2|^2$ blue) (d) for full charging in minimum time, when $\Omega_0/J = 6$ and $\chi = J'/\Omega_z = 2$.

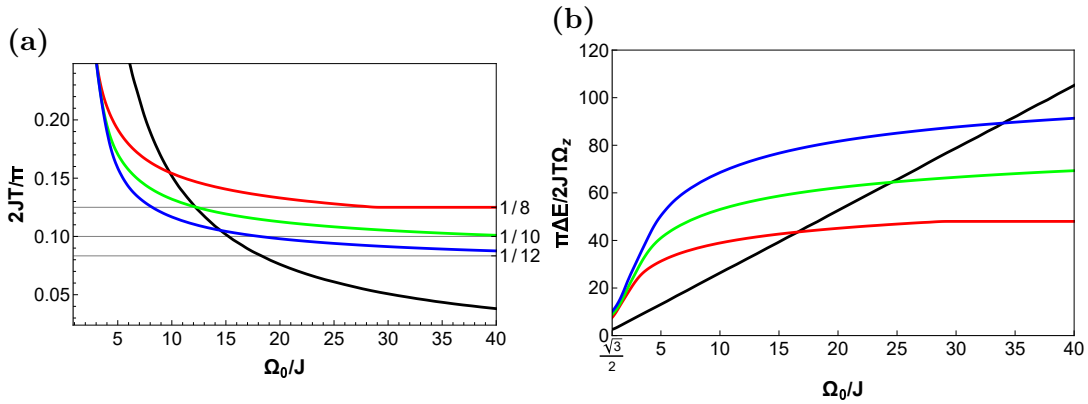

Figure 10: Minimum duration for full charging (a) and achieved charging power $\Delta E_{max}/T$ (b) as functions of parameter Ω_0/J, for the case $J < \Omega_z$ (black solid line) and the case $J' > \Omega_z$ with different values of $J'/J = 4, 5, 6$ (red, green, and blue solid lines, respectively).

$$c_1(T) = e^{-i\phi_1}\left\{-\frac{1}{2}\sin\theta_1\sin\theta_3[e^{i\delta\phi} + e^{-i(\delta\phi+\theta_2)}] + \cos\theta_1\cos\theta_3\right\}, \tag{36}$$

$$c_2(T) = \frac{ie^{-i(\phi_1+\phi_2)}}{\sqrt{2}}\left\{-\frac{1}{2}\sin\theta_1(1+\cos\theta_3)e^{i\delta\phi} + \frac{1}{2}\sin\theta_1(1-\cos\theta_3)e^{-i(\delta\phi+\theta_2)} - \cos\theta_1\sin\theta_3\right\}.$$

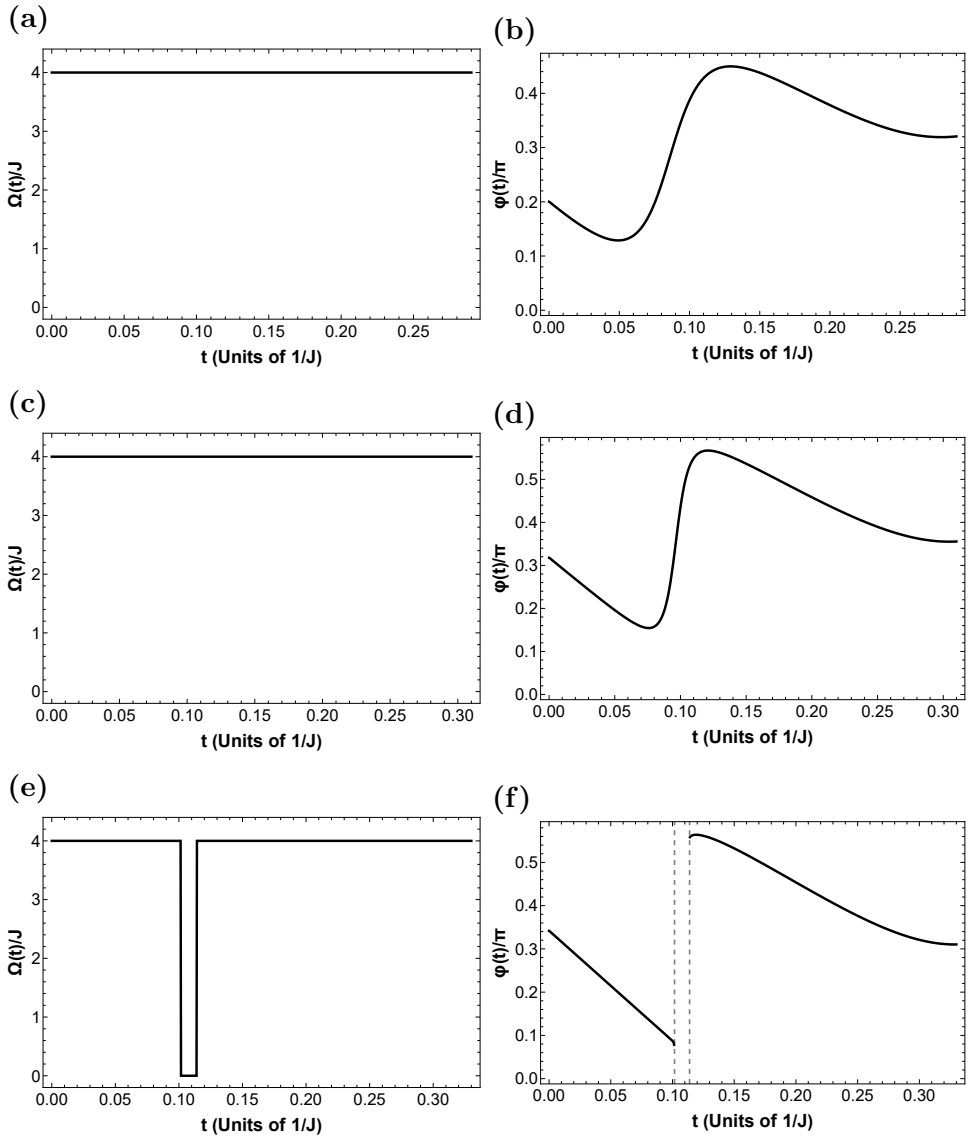

Figure 11: Optimal control amplitude (first column) and phase (second column) when $\Omega_0/J = 4$ and $\chi = J'/\Omega_z = 2$, for charging duration $T = 0.29J^{-1}$ (a, b), $T = 0.31J^{-1}$ (c, d), and $T = 0.33J^{-1}$ (e, f).

For full charging of the battery it is necessary that $c_0(T) = c_1(T) = 0$. These equations form a linear system for $e^{i\delta\phi}$ and $e^{-i(\delta\phi+\theta_2)}$ which can be easily solved to give

$$e^{i\theta_2} = -\tan^2\theta_1, \tag{37a}$$

$$e^{i\delta\phi} = \cot\theta_1 \cot\frac{\theta_3}{2}. \tag{37b}$$

From Eq. (37a) it is $\sin\theta_2 = 0$ and since $\cos\theta_2 = -\tan^2\theta_1 < 0$ we get $\theta_2 = \pi$ and consequently $\theta_1 = \pi/4$. Using this last value in Eq. (37b) we have $\sin\delta\phi = 0$ and $\cos\delta\phi = \cot\frac{\theta_3}{2}$. For $\delta\phi = 0$ the smallest positive solution $\theta_3 = \pi/2$ is obtained. We

have thus found that for full charging

$$\theta_1 = \frac{\pi}{4}, \quad \theta_2 = \pi, \quad \theta_3 = \frac{\pi}{2}. \tag{38}$$

The initial and final delta pulses do not contribute to the pulse-sequence duration, which is solely determined by angle θ_2. Thus, in the limit $\Omega_0 \to \infty$, the minimum duration for full charging tends to

$$T \to \frac{\pi}{4J'}. \tag{39}$$

For $J'/J = 4, 5, 6$, we recover the limits shown on the right of Fig. 10(a).

5. Singular control and dynamical Lie algebra

In this section we will use the dynamical Lie algebras generated by the corresponding Hamiltonians in Eqs. (14) and (30), in an attempt to understand why the singular control $\Omega(t) = 0$ appears in the optimal pulse sequence only in the latter case and not in the former. Since in both cases we effectively deal with a three-level system, we will use as a basis of $su(3)$ the Gell-Mann matrices given below,

$$\begin{aligned}
\hat{\Lambda}_0 &= \frac{2}{3}\begin{bmatrix} 1 & 0 & 0 \\ 0 & 1 & 0 \\ 0 & 0 & 1 \end{bmatrix}, \qquad \hat{\Lambda}_1 = \begin{bmatrix} 0 & 1 & 0 \\ 1 & 0 & 0 \\ 0 & 0 & 0 \end{bmatrix}, \qquad \hat{\Lambda}_2 = \begin{bmatrix} 0 & -i & 0 \\ i & 0 & 0 \\ 0 & 0 & 0 \end{bmatrix}, \\
\hat{\Lambda}_3 &= \begin{bmatrix} 1 & 0 & 0 \\ 0 & -1 & 0 \\ 0 & 0 & 0 \end{bmatrix}, \qquad \hat{\Lambda}_4 = \begin{bmatrix} 0 & 0 & 1 \\ 0 & 0 & 0 \\ 1 & 0 & 0 \end{bmatrix}, \qquad \hat{\Lambda}_5 = \begin{bmatrix} 0 & 0 & -i \\ 0 & 0 & 0 \\ i & 0 & 0 \end{bmatrix}, \\
\hat{\Lambda}_6 &= \begin{bmatrix} 0 & 0 & 0 \\ 0 & 0 & 1 \\ 0 & 1 & 0 \end{bmatrix}, \qquad \hat{\Lambda}_7 = \begin{bmatrix} 0 & 0 & 0 \\ 0 & 0 & -i \\ 0 & i & 0 \end{bmatrix}, \qquad \hat{\Lambda}_8 = \frac{1}{3}\begin{bmatrix} 1 & 0 & 0 \\ 0 & 1 & 0 \\ 0 & 0 & -2 \end{bmatrix},
\end{aligned} \tag{40}$$

where note that we have used capital lambda instead of the usually employed lower case letters, to avoid the confusion with the adjoint variables. We will use the following real-valued quantities related to the Gell-Mann matrices ($i = 1, 2, \ldots, 8$)

$$\Lambda_i = \Re\Big\{-i \langle\lambda|\hat{\Lambda}_i|\psi\rangle\Big\}, \tag{41}$$

and specifically their time evolution given from the relation

$$\dot{\Lambda}_i = \Re\Big\{\langle\lambda|\left[\hat{H}, \hat{\Lambda}_i\right]|\psi\rangle\Big\}, \tag{42}$$

which is easily derived using Eqs. (8) and (21) for the state and adjoint vectors. Note that the commutator $\left[\hat{H}, \hat{\Lambda}_i\right]$ generates the dynamical Lie algebra corresponding to Hamiltonian $\hat{H}$, the Hermitian matrix on the right hand side of Eq. (14) or (30), depending on the case. We will also use the following notation for the controls

$$u_x(t) = \sqrt{2}\Omega(t)\cos\phi(t), \tag{43a}$$

$$u_y(t) = \sqrt{2}\Omega(t)\sin\phi(t), \tag{43b}$$

for better tracking of the equations.

5.1. Case $J > \Omega_z$

We start from the case where the singular control $\Omega(t) = 0$ enters the optimal solution. The Hamiltonian from Eq. (30) can be expressed in terms of the Gell-Manm matrices as

$$\hat{H} = u_x \left(\hat{\Lambda}_1 + \hat{\Lambda}_6\right) - u_y \left(\hat{\Lambda}_2 + \hat{\Lambda}_7\right) + 2J \left(\hat{\Lambda}_0 + \hat{\Lambda}_3 + \hat{\Lambda}_8\right) \tag{44}$$

Using this relation in Eq. (42), along with the commutation relations of the Gell-Mann matrices and definition (41), we obtain the following system for Λ_i

$$\dot{\Lambda}_1 = 4J\Lambda_2 - u_x\Lambda_5 + u_y(2\Lambda_3 - \Lambda_4), \tag{45a}$$
$$\dot{\Lambda}_2 = -4J\Lambda_1 + u_x(2\Lambda_3 + \Lambda_4) - u_y\Lambda_5, \tag{45b}$$
$$\dot{\Lambda}_3 = u_x(\Lambda_7 - 2\Lambda_2) + u_y(\Lambda_6 - 2\Lambda_1), \tag{45c}$$
$$\dot{\Lambda}_4 = 4J\Lambda_5 + u_x(\Lambda_7 - \Lambda_2) + u_y(\Lambda_1 - \Lambda_6), \tag{45d}$$
$$\dot{\Lambda}_5 = -4J\Lambda_4 + u_x(\Lambda_1 - \Lambda_6) + u_y(\Lambda_2 - \Lambda_7), \tag{45e}$$
$$\dot{\Lambda}_6 = u_x\Lambda_5 - u_y(\Lambda_3 - \Lambda_4 - 3\Lambda_8), \tag{45f}$$
$$\dot{\Lambda}_7 = -u_x(\Lambda_3 + \Lambda_4 - 3\Lambda_8) + u_y\Lambda_5, \tag{45g}$$
$$\dot{\Lambda}_8 = -u_x\Lambda_7 - u_y\Lambda_6. \tag{45h}$$

The control Hamiltonian can be expressed as

$$H_c = \Re(\langle\lambda|\dot{\psi}\rangle) = \Re(-i\,\langle\lambda|\hat{H}|\psi\rangle) = u_xB + u_yA + JC, \tag{46}$$

where

$$A = -(\Lambda_2 + \Lambda_7), \tag{47a}$$
$$B = \Lambda_1 + \Lambda_6, \tag{47b}$$
$$C = 2(\Lambda_0 + \Lambda_3 + \Lambda_8). \tag{47c}$$

From the analysis of section 3 we have that, when $A \neq 0$ or $B \neq 0$, the optimal controls are given by the relations

$$u_x^* = \sqrt{2}\Omega_0 \cos\phi^* = \sqrt{2}\Omega_0 \frac{B}{\sqrt{A^2 + B^2}}, \tag{48a}$$
$$u_y^* = \sqrt{2}\Omega_0 \sin\phi^* = \sqrt{2}\Omega_0 \frac{A}{\sqrt{A^2 + B^2}}. \tag{48b}$$

In the singular case where $A = B = 0$ for a finite time interval, it also holds

$$\dot{A} = 4J\Lambda_1 - u_x\,(\Lambda_3 + 3\Lambda_8) = 0, \tag{49a}$$
$$\dot{B} = 4J\Lambda_2 + u_y\,(\Lambda_3 + 3\Lambda_8) = 0. \tag{49b}$$

The coefficient Λ_3+$3\Lambda_8$ multiplying both controls in Eqs. (49a), (49b) obeys the equation

$$\dot{\Lambda}_3 + 3\dot{\Lambda}_8 = -2u_x(\Lambda_2 + \Lambda_7) - 2u_y(\Lambda_1 + \Lambda_6) = 2(u_xA - u_yB) \tag{50}$$

It is not hard to see that the right hand side of Eq. (50) is always zero, trivially when $A = B = 0$, while for $A \neq 0$ or $B \neq 0$ because of Eqs. (48a), (48b). This implies that $\Lambda_3 + 3\Lambda_8$ is constant throughout and equal to its value at $t = 0$

$$\Lambda_3(t) + 3\Lambda_8(t) = \Lambda_3(0) + 3\Lambda_8(0) = 0, \tag{51}$$

where the initial value is zero because $\hat{\Lambda}_3 + 3\hat{\Lambda}_8 = \mathrm{diag}(2\ 0\ -2)$ and the starting state is $|\psi(0)\rangle = |\psi_1\rangle = (0,1,0)^T$. Using Eq. (51) in Eqs. (49a), (49b) we get on the singular interval that $\Lambda_1 = \Lambda_2 = 0$ and thus

$$\dot{\Lambda}_1 = (2\Lambda_3 - \Lambda_4)\, u_y - \Lambda_5 u_x = 0, \tag{52a}$$

$$\dot{\Lambda}_2 = (2\Lambda_3 + \Lambda_4)\, u_x - \Lambda_5 u_y = 0. \tag{52b}$$

Excluding the special case where $\Lambda_4^2 + \Lambda_5^2 = 4\Lambda_3^2$, the only solution to the homogeneous system (52a), (52b) is the trivial one $u_x = 0, u_y = 0$, leading to $\Omega(t) = 0$ along the singular arc. Note that zero singular controls also arise in the time-optimal selective control of two *uncoupled* spins-1/2 [67].

5.2. Case $J < \Omega_z$

Here we examine what is different compared to the previous case and there is no interval where $\Omega(t) = 0$ in the optimal solution. The Hamiltonian from Eq. (14) can be expressed in terms of the Gell-Manm matrices as

$$\hat{H} = u_x\,(\Lambda_1 + \Lambda_6) - u_y\,(\Lambda_2 + \Lambda_7) - J\,(\Lambda_0 - \Lambda_3 + \Lambda_8)\,, \tag{53}$$

leading to the following system for Λ_i

$$\dot{\Lambda}_1 = 2J\Lambda_2 - u_x\Lambda_5 + u_y(2\Lambda_3 - \Lambda_4), \tag{54a}$$

$$\dot{\Lambda}_2 = -2J\Lambda_1 + u_x(2\Lambda_3 + \Lambda_4) - u_y\Lambda_5, \tag{54b}$$

$$\dot{\Lambda}_3 = u_x(\Lambda_7 - 2\Lambda_2) + u_y(\Lambda_6 - 2\Lambda_1), \tag{54c}$$

$$\dot{\Lambda}_4 = u_x(\Lambda_7 - \Lambda_2) + u_y(\Lambda_1 - \Lambda_6), \tag{54d}$$

$$\dot{\Lambda}_5 = u_x(\Lambda_1 - \Lambda_6) + u_y(\Lambda_2 - \Lambda_7), \tag{54e}$$

$$\dot{\Lambda}_6 = -2J\Lambda_7 + u_x\Lambda_5 - u_y(\Lambda_3 - \Lambda_4 - 3\Lambda_8), \tag{54f}$$

$$\dot{\Lambda}_7 = 2J\Lambda_6 - u_x(\Lambda_3 + \Lambda_4 - 3\Lambda_8) + u_y\Lambda_5, \tag{54g}$$

$$\dot{\Lambda}_8 = -u_x\Lambda_7 - u_y\Lambda_6. \tag{54h}$$

The control Hamiltonian can be written as in Eq. (46), with A, B given in Eqs. (47a), (47b), while here

$$C = -\Lambda_0 + \Lambda_3 - \Lambda_8. \tag{55}$$

Similarly to the previous case, when $A = B = 0$ we also get

$$\dot{A} = 2J\,(\Lambda_1 - \Lambda_6) - u_x\,(\Lambda_3 + 3\Lambda_8) = 0, \tag{56a}$$

$$\dot{B} = 2J\,(\Lambda_2 - \Lambda_7) + u_y\,(\Lambda_3 + 3\Lambda_8) = 0. \tag{56b}$$

The control coefficient $\Lambda_3 + 3\Lambda_8$ obeys Eq. (50) and using the same reasoning as before it turns out to be constant throughout. The difference compared to the previous case is that here the starting state is $|\psi(0)\rangle = |\psi_0\rangle = (1,0,0)^T$, thus we cannot infer that $\Lambda_3(t) + 3\Lambda_8(t) = 0$ and apply the arguments used before.

6. Conclusion

We studied a quantum battery consisting of an Ising pair of coupled spins$-1/2$ in the standard NMR framework, with constant longitudinal field and a control transverse field with time-dependent amplitude and phase, using optimal control to find rapid charging protocols. We investigated two configurations, with the Ising interaction being weaker and stronger than the longitudinal field. In the first configuration, the spin-down state has the lowest energy and the corresponding optimal charging protocol specifies a constant transverse field amplitude equal to its maximum bound, while the minimum time needed for full charging of the battery tends to zero with increasing bound. In the second configuration, a maximally entangled Bell state has the lowest energy and the corresponding optimal charging protocol includes a time interval where the transverse field amplitude is zero and its phase is irrelevant, connected to singular control. In this configuration, higher levels of stored energy can be reached, while the minimum time for full charging attains a nonzero limiting value proportional to the inverse Ising coupling, with increasing maximum bound of the control amplitude. We examined intuitively and quantitatively the dissimilar behavior in the two configurations and furthermore used the dynamical Lie algebra of the quantum system to better understand the presence of a singular arc in the optimal pulse-sequence in the second situation. The interplay found between the quantum system parameters, the stored energy and the minimum charging duration, provides many possibilities for optimizing the operation of quantum battery under various constraints. We thus expect the present work to find applications in this emerging field of modern quantum science and technology, and we work towards extending it to larger spin chains.

Acknowledgments

The present work was financially supported by the "Andreas Mentzelopoulos Foundation".

References

[1] Alicki R and Fannes M 2013 *Phys. Rev. E* **87**(4) 042123 URL https://link.aps.org/doi/10.1103/PhysRevE.87.042123

[2] Campaioli F, Gherardini S, Quach J Q, Polini M and Andolina G M 2024 *Rev. Mod. Phys.* **96**(3) 031001 URL https://link.aps.org/doi/10.1103/RevModPhys.96.031001

[3] Binder F C, Vinjanampathy S, Modi K and Goold J 2015 *New Journal of Physics* **17** 075015 URL https://dx.doi.org/10.1088/1367-2630/17/7/075015

[4] Rossini D, Andolina G M, Rosa D, Carrega M and Polini M 2020 *Phys. Rev. Lett.* **125**(23) 236402 URL https://link.aps.org/doi/10.1103/PhysRevLett.125.236402

[5] Gyhm J Y, Šafránek D and Rosa D 2022 *Phys. Rev. Lett.* **128**(14) 140501 URL https://link.aps.org/doi/10.1103/PhysRevLett.128.140501

[6] Campaioli F, Pollock F A, Binder F C, Céleri L, Goold J, Vinjanampathy S and Modi K 2017 *Phys. Rev. Lett.* **118**(15) 150601 URL https://link.aps.org/doi/10.1103/PhysRevLett.118.150601

[7] Gyhm J Y and Fischer U R 2024 *AVS Quantum Science* **6** 012001 ISSN 2639-0213 (*Preprint* https://pubs.aip.org/avs/aqs/article-pdf/doi/10.1116/5.0184903/18703178/012001_1_5.01 URL https://doi.org/10.1116/5.0184903

[8] Andolina G M, Farina D, Mari A, Pellegrini V, Giovannetti V and Polini M 2018 *Phys. Rev. B* **98**(20) 205423 URL https://link.aps.org/doi/10.1103/PhysRevB.98.205423

[9] Le T P, Levinsen J, Modi K, Parish M M and Pollock F A 2018 *Phys. Rev. A* **97**(2) 022106 URL https://link.aps.org/doi/10.1103/PhysRevA.97.022106

[10] Zhang Y Y, Yang T R, Fu L and Wang X 2019 *Phys. Rev. E* **99**(5) 052106 URL https://link.aps.org/doi/10.1103/PhysRevE.99.052106

[11] Barra F 2019 *Phys. Rev. Lett.* **122**(21) 210601 URL https://link.aps.org/doi/10.1103/PhysRevLett.122.210601

[12] Santos A C, Çakmak B i e i f m c, Campbell S and Zinner N T 2019 *Phys. Rev. E* **100**(3) 032107 URL https://link.aps.org/doi/10.1103/PhysRevE.100.032107

[13] Andolina G M, Keck M, Mari A, Campisi M, Giovannetti V and Polini M 2019 *Phys. Rev. Lett.* **122**(4) 047702 URL https://link.aps.org/doi/10.1103/PhysRevLett.122.047702

[14] Crescente A, Carrega M, Sassetti M and Ferraro D 2020 *Phys. Rev. B* **102**(24) 245407 URL https://link.aps.org/doi/10.1103/PhysRevB.102.245407

[15] Santos A C, Saguia A and Sarandy M S 2020 *Phys. Rev. E* **101**(6) 062114 URL https://link.aps.org/doi/10.1103/PhysRevE.101.062114

[16] Santos A C 2021 *Phys. Rev. E* **103**(4) 042118 URL https://link.aps.org/doi/10.1103/PhysRevE.103.042118

[17] Carrasco J, Maze J R, Hermann-Avigliano C and Barra F 2022 *Phys. Rev. E* **105**(6) 064119 URL https://link.aps.org/doi/10.1103/PhysRevE.105.064119

[18] Dou F Q, Lu Y Q, Wang Y J and Sun J A 2022 *Phys. Rev. B* **105**(11) 115405 URL https://link.aps.org/doi/10.1103/PhysRevB.105.115405

[19] Barra F, Hovhannisyan K V and Imparato A 2022 *New Journal of Physics* **24** 015003 URL https://dx.doi.org/10.1088/1367-2630/ac43ed

[20] Shaghaghi V, Singh V, Benenti G and Rosa D 2022 *Quantum Science and Technology* **7** 04LT01 URL https://dx.doi.org/10.1088/2058-9565/ac8829

[21] Rodríguez C, Rosa D and Olle J 2023 *Phys. Rev. A* **108**(4) 042618 URL https://link.aps.org/doi/10.1103/PhysRevA.108.042618

[22] Kamin F, Abuali Z, Ness H and Salimi S 2023 *JOURNAL OF PHYSICS A MATHEMATICAL AND GENERAL* **56** ISSN 0305-4470 funding Information: S Salimi thanks research funded by Iran national science foundation (INSF) under Project No. 4003162. Publisher Copyright: © 2023 IOP Publishing Ltd.

[23] Downing C A and Ukhtary M S 2023 *Communications Physics* **6** 322 ISSN 2399-3650 URL https://doi.org/10.1038/s42005-023-01439-y

[24] Hadipour M, Haseli S, Wang D and Haddadi S 2023 Practical scheme for realization of a quantum battery (*Preprint* 2312.06389)

[25] Kamin F H, Tabesh F T, Salimi S and Santos A C 2020 *Phys. Rev. E* **102**(5) 052109 URL https://link.aps.org/doi/10.1103/PhysRevE.102.052109

[26] Pirmoradian F and Mølmer K 2019 *Phys. Rev. A* **100**(4) 043833 URL https://link.aps.org/doi/10.1103/PhysRevA.100.043833

[27] Zhang X and Blaauboer M 2023 *Frontiers in Physics* **10** ISSN 2296-424X URL https://www.frontiersin.org/articles/10.3389/fphy.2022.1097564

[28] Crescente A, Carrega M, Sassetti M and Ferraro D 2020 *New Journal of Physics* **22** 063057 URL https://doi.org/10.1088/1367-2630/ab91fc

[29] Joshi J and Mahesh T S 2022 *Phys. Rev. A* **106**(4) 042601 URL https://link.aps.org/doi/10.1103/PhysRevA.106.042601

[30] Mohan B and Pati A K 2021 *Phys. Rev. A* **104**(4) 042209 URL https://link.aps.org/doi/10.1103/PhysRevA.104.042209

[31] Niedenzu W, Mukherjee V, Ghosh A, Kofman A G and Kurizki G 2018 *Nature Communications* **9** 165 URL https://doi.org/10.1038/s41467-017-01991-6

[32] Ferraro D, Campisi M, Andolina G M, Pellegrini V and Polini M 2018 *Phys. Rev. Lett.* **120**(11) 117702 URL https://link.aps.org/doi/10.1103/PhysRevLett.120.117702

[33] Zhao F, Dou F Q and Zhao Q 2021 *Phys. Rev. A* **103**(3) 033715 URL https://link.aps.org/doi/10.1103/PhysRevA.103.033715

[34] Rossini D, Andolina G M and Polini M 2019 *Phys. Rev. B* **100**(11) 115142 URL https://link.aps.org/doi/10.1103/PhysRevB.100.115142

[35] Zakavati S, Tabesh F T and Salimi S 2021 *Phys. Rev. E* **104**(5) 054117 URL https://link.aps.org/doi/10.1103/PhysRevE.104.054117

[36] Zhao F, Dou F Q and Zhao Q 2022 *Phys. Rev. Res.* **4**(1) 013172 URL https://link.aps.org/doi/10.1103/PhysRevResearch.4.013172

[37] Hu C K, Qiu J, Souza P J P, Yuan J, Zhou Y, Zhang L, Chu J, Pan X, Hu L, Li J, Xu Y, Zhong Y, Liu S, Yan F, Tan D, Bachelard R, Villas-Boas C J, Santos A C and Yu D 2022 *Quantum Science and Technology* **7** 045018 URL https://dx.doi.org/10.1088/2058-9565/ac8444

[38] Maillette de Buy Wenniger I, Thomas S E, Maffei M, Wein S C, Pont M, Belabas N, Prasad S, Harouri A, Lemaître A, Sagnes I, Somaschi N,

Auffèves A and Senellart P 2023 *Phys. Rev. Lett.* **131**(26) 260401 URL https://link.aps.org/doi/10.1103/PhysRevLett.131.260401

[39] Quach J Q, McGhee K E, Ganzer L, Rouse D M, Lovett B W, Gauger E M, Keeling J, Cerullo G, Lidzey D G and Virgili T 2022 *Science Advances* **8** eabk3160 (*Preprint* https://www.science.org/doi/pdf/10.1126/sciadv.abk3160) URL https://www.science.org/doi/abs/10.1126/sciadv.abk3160

[40] Dou F Q, Wang Y J and Sun J A 2020 *Europhysics Letters* **131** 43001 URL https://dx.doi.org/10.1209/0295-5075/131/43001

[41] Moraes L F C, Saguia A, Santos A C and Sarandy M S 2022 *Europhysics Letters* **136** 23001 URL https://dx.doi.org/10.1209/0295-5075/ac1363

[42] Dou F Q, Wang Y J and Sun J A 2021 *Frontiers of Physics* **17** 31503 ISSN 2095-0470 URL https://doi.org/10.1007/s11467-021-1130-5

[43] Dou F Q, Wang Y J and Sun J A 2022 Charging advantages of lipkin-meshkov-glick quantum battery (*Preprint* 2208.04831)

[44] Guo W X, Yang F M and Dou F Q 2024 *Phys. Rev. A* **109**(3) 032201 URL https://link.aps.org/doi/10.1103/PhysRevA.109.032201

[45] Yang F M and Dou F Q 2024 *Phys. Rev. A* **109**(6) 062432 URL https://link.aps.org/doi/10.1103/PhysRevA.109.062432

[46] Mazzoncini F, Cavina V, Andolina G M, Erdman P A and Giovannetti V 2023 *Phys. Rev. A* **107**(3) 032218 URL https://link.aps.org/doi/10.1103/PhysRevA.107.032218

[47] Evangelakos V, Paspalakis E and Stefanatos D 2024 *Phys. Rev. A* **110**(5) 052601 URL https://link.aps.org/doi/10.1103/PhysRevA.110.052601

[48] Rodríguez R R, Ahmadi B, Suárez G, Mazurek P, Barzanjeh S and Horodecki P 2024 *New Journal of Physics* **26** 043004 URL https://dx.doi.org/10.1088/1367-2630/ad3843

[49] Erdman P A, Andolina G M, Giovannetti V and Noé F 2024 *Phys. Rev. Lett.* **133**(24) 243602 URL https://link.aps.org/doi/10.1103/PhysRevLett.133.243602

[50] Sun P Y, Zhou H and Dou F Q 2024 Cavity-heisenberg spin-j chain quantum battery and reinforcement learning optimization (*Preprint* 2412.01442) URL https://arxiv.org/abs/2412.01442

[51] Stefanatos D and Paspalakis E 2021 *Europhysics Letters* **132** 60001 URL https://dx.doi.org/10.1209/0295-5075/132/60001

[52] Král P, Thanopulos I and Shapiro M 2007 *Rev. Mod. Phys.* **79**(1) 53–77 URL https://link.aps.org/doi/10.1103/RevModPhys.79.53

[53] Vitanov N V, Rangelov A A, Shore B W and Bergmann K 2017 *Rev. Mod. Phys.* **89**(1) 015006 URL https://link.aps.org/doi/10.1103/RevModPhys.89.015006

[54] Guéry-Odelin D, Ruschhaupt A, Kiely A, Torrontegui E, Martínez-Garaot S and Muga J G 2019 *Rev. Mod. Phys.* **91**(4) 045001 URL https://link.aps.org/doi/10.1103/RevModPhys.91.045001

[55] Deffner S and Campbell S 2017 *Journal of Physics A: Mathematical and Theoretical* **50** 453001 URL https://dx.doi.org/10.1088/1751-8121/aa86c6

[56] Shrimali D, Panda B and Pati A K 2024 *Phys. Rev. A* **110**(2) 022425 URL https://link.aps.org/doi/10.1103/PhysRevA.110.022425

[57] Pontryagin L S, Boltyanskii V G, Gamkrelidze R V and Mishchenko E F 1962 *The Mathematical Theory of Optimal Processes* (Interscience Publishers)

[58] Schättler H and Ledzewicz U 2012 *Geometric Optimal Control: Theory, Methods and Examples* (Springer New York, NY) ISBN 978-1-4614-3833-5 URL https://doi.org/10.1007/978-1-4614-3834-2

[59] Stefanatos D 2009 *Phys. Rev. A* **80**(4) 045401 URL https://link.aps.org/doi/10.1103/PhysRevA.80.045401

[60] Boscain U, Sigalotti M and Sugny D 2021 *PRX Quantum* **2**(3) 030203 URL https://link.aps.org/doi/10.1103/PRXQuantum.2.030203

[61] Lokutsievskiy L V, Pechen A N and Zelikin M I 2024 *Journal of Physics A: Mathematical and Theoretical* **57** 275302 URL https://dx.doi.org/10.1088/1751-8121/ad5396

[62] Koutromanos D, Stefanatos D and Paspalakis E 2025 *Computer Physics Communications* **310** 109505 ISSN 0010-4655 URL https://www.sciencedirect.com/science/article/pii/S0010465525000086

[63] Stojanović V M and Nauth J K 2023 *Phys. Rev. A* **108**(1) 012608 URL https://link.aps.org/doi/10.1103/PhysRevA.108.012608

[64] Unanyan R G, Vitanov N V and Bergmann K 2001 *Phys. Rev. Lett.* **87**(13) 137902 URL https://link.aps.org/doi/10.1103/PhysRevLett.87.137902

[65] Stefanatos D and Paspalakis E 2020 *Phys. Rev. A* **102**(5) 052618 URL https://link.aps.org/doi/10.1103/PhysRevA.102.052618

[66] Ansel Q, Dionis E, Arrouas F, Peaudecerf B, Guérin S, Guéry-Odelin D and Sugny D 2024 *Journal of Physics B: Atomic, Molecular and Optical Physics* **57** 133001 URL https://dx.doi.org/10.1088/1361-6455/ad46a5

[67] Van Damme L, Ansel Q, Glaser S J and Sugny D 2018 *Phys. Rev. A* **98**(4) 043421 URL https://link.aps.org/doi/10.1103/PhysRevA.98.043421